FDTD Modeling of Nonlinear Phenomena in Wave Transmission Through Graphene

Liang Yang, Jing Tian, Khalid Z. Rajab, *Member, IEEE*, and Yang Hao, *Fellow, IEEE*

***Abstract*—A novel finite-difference time-domain modeling method is proposed to simulate the nonlinear electrodynamic responses of graphene at terahertz frequencies. The relation between currents in graphene and electromagnetic waves is governed by a J–E characteristic formula at the frequencies where the conductivity of graphene exhibits resonant behavior. Simulation results demonstrate nonlinear phenomena in wave transmission through graphene including odd-harmonic generation and frequency-mixing effect. The proposed modeling method can be used as a full-wave solution to the design of nonlinear graphene-based structures.**

***Index Terms*—Finite-difference time-domain (FDTD) method, graphene, nonlinearity.**

I. Introduction

GRAPHENE, a two-dimensional material with interesting electromagnetic (EM) properties, has inspired researchers to propose linear graphene-based devices such as reflector [1], absorber [2], and isolator [3]. On the other hand, graphene also owns promising nonlinear properties.

The band structure of graphene exhibits a linear energy dispersion relation near its Dirac points [4]. This linear band structure can theoretically lead to the suppression of ac electric current in graphene, and hence it results in the generation of odd harmonics under strong terahertz (THz) field illumination [5]. It has been predicted in [6] that a THz field with a peak value of 1 kV/cm is capable of inducing third-order harmonic generation (THG) on monolayer graphene at room temperature. The amplitude of generated third-order harmonic can be tuned by varying the Fermi level of graphene with bias voltage [7]. To maximize THG, the optimized relation between incident field amplitudes and Fermi levels has been discussed in [8]. Further enhancement can also be achieved by utilizing appropriate graphene-dielectric-metal structures [9]. The third-order conductivity of graphene with resonant behavior at THz has been proposed in [10] to analyze various nonlinear phenomena. As isolated graphene is a centrosymmetric material, the even-order harmonic generation is forbidden, leaving only odd-order harmonic excitations [11]. In addition, the effects of magnetic bias on the nonlinearity of graphene are also investigated [12]. In terms of experiments, high THz field excitations with peak electric fields between 0.2 and 63 kV/cm have been used to explore the nonlinear properties of graphene. The odd-harmonic generation of graphene has been verified experimentally using a 45-layer graphene sample [13]. Moreover, the nonlinear transmission enhancement of photoexcited monolayer graphene has also been reported in [14], enabling the realization of graphene-based tunable nonlinear devices.

The finite-difference time-domain (FDTD) method is a useful full-wave numerical approach, which is frequently used to assist with EM device design. The applications of FDTD methods for simulating magnetic and electric nonlinearities of other materials have been discussed [15]–[19]. The magnetic nonlinearity is modeled through updating magnetic fields with a differential permeability derived from the B–H characteristic formula [15]. Although this approach has been successfully implemented to simulate the pulse propagation through nonlinear magnetic sheets, the fine mesh required by the geometric details of magnetic sheets leads to very small time-steps [16]. In terms of electric nonlinearity, a single time convolution approach has been used to analyze both Kerr and Raman interactions [17]. As this model considers the case of non-resonant third-order processes [18], it is only suitable for optical spectra where graphene does not exhibit resonant nonlinear behavior [20]. In addition, the numerical simulation of anisotropic materials with frequency-independent nonlinear constants has been discussed in [19] as well. To model graphene that has a frequency-dependent conductivity at THz, complex time-domain convolution is required in their FDTD updating equations. Recently, an FDTD method for modeling the THz nonlinearity of graphene was also proposed. The nonlinearity of graphene is represented as a time-domain instantaneous conductivity $\sigma(t) = \mathbf{J}(t)/\mathbf{E}(t)$, resulting in even-order harmonic excitation in their simulation results [21].

In this letter, a new FDTD method is proposed to simulate the THz nonlinearity of graphene under strong THz field illumination. The updating equation is directly obtained from the characteristic formula derived in [5], hence the explicit expression of graphene conductivity is not required and the complex time-domain convolution is also avoided. The excitation of odd-order harmonics is successfully demonstrated, and the frequency mixing of two THz signals is also presented.

II. FDTD Modeling

Assuming that the thermal energy is much less than the chemical potential of graphene, the surface current $\mathbf{J}_s(t)$ of graphene derived from the quasi-classical kinetic theory can be

Manuscript received September 12, 2017; revised October 30, 2017; accepted November 15, 2017. Date of publication December 11, 2017; date of current version January 10, 2018. This work was supported in part by the China Scholarship Council, in part by the Engineering and Physical Sciences Research Council under Grant EP/K01711X/1, in part by the EU Graphene Flagship under Grant FP7-ICT-604391, and in part by the Graphene Core 1 under Grant H2020 696656. *(Corresponding author: Yang Hao.)*

The authors are with the School of Electronic Engineering and Computer Science, Queen Mary University of London, London E1 4NS, U.K. (e-mail: liang.yang@qmul.ac.uk; j.tian@qmul.ac.uk; k.rajab@qmul.ac.uk; y.hao@qmul.ac.uk).

Digital Object Identifier 10.1109/LAWP.2017.2777530

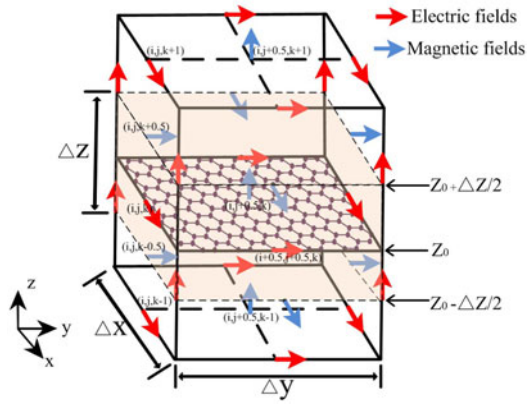

Fig. 1. Yee cells in FDTD with a graphene sheet in xy plane. The Yee cell where the graphene sheet exists is filled with light color. Red (blue) arrows represent electric (magnetic) fields. Δx, Δy, and Δz are cell sizes in the three directions.

approximately expressed as [5]

$$\mathbf{J}_s(t) = \frac{ev_F p_F^2 \mathbf{P}(t)}{\pi\hbar^2\sqrt{1+P^2(t)}} G\left(Q(t)\right) \tag{1}$$

where e is the charge of an electron, v_F is the Fermi velocity of graphene, $p_F = \mu/v_F$ is the Fermi momentum, μ is the chemical potential, $\mathbf{P}(t) = e\mathbf{A}(t)/p_F$ is the dimensionless vector variable, $P(t) = |\mathbf{P}(\mathbf{t})|$, $\mathbf{A}(t) = \int_0^t \mathbf{E}(t')dt'$ is the vector potential, $\mathbf{E}(t)$ is the in-plane electric field, $\hbar$ is the reduced Planck constant, and $G\left(Q(t)\right)$ is approximated as

$$G\left(Q(t)\right) \approx 1 + \frac{3}{32}Q^2(t) + \frac{35}{1024}Q^4(t) \tag{2}$$

where $Q(t) = 2P(t)/(1+P^2(t))$.

Equation (1) is a J–E characteristic formula describing the strong $\mathbf{E}(t)$ induced $\mathbf{J}_s(t)$ at THz frequency. As it ignores the interband transitions, (1) is only suitable for the THz region where the intraband transitions dominate.

For an isotropic graphene sheet oriented in the xy plane, as shown in Fig. 1, the time-domain Maxwell equation including the surface currents of graphene can be expressed as

$$\varepsilon\frac{\partial\mathbf{E}(t)}{\partial t} = \nabla\times\mathbf{H}(t) - \mathbf{J}_s(t)\delta(z-z_0) \tag{3}$$

where ε is the average permittivity of materials surrounding graphene, and $\delta(z)$ is the Dirac delta function with z_0 representing the position of graphene.

By taking the difference between time-step n and $n+1$ on the E_x component and integrating both sides of (3) from $z_0 - \Delta z/2$ to $z_0 + \Delta z/2$ [22], the following updating equation can be obtained:

$$\begin{aligned} &E_x^{n+1}(i,j,k) \\ &\quad = E_x^n(i,j,k) \\ &\qquad + \frac{\Delta t}{\varepsilon}\left[\frac{H_z^{n+0.5}(i,j+0.5,k) - H_z^{n+0.5}(i,j-0.5,k)}{\Delta y}\right. \\ &\qquad\quad - \frac{H_y^{n+0.5}(i,j,k+0.5) - H_y^{n+0.5}(i,j,k-0.5)}{\Delta z} \\ &\qquad\quad \left. - \frac{J_{sx}^{n+0.5}(i,j,k)}{\Delta z}\right] \end{aligned} \tag{4}$$

where (i,j,k) represent the position index of a field variable, Δt is the time-step, and n is a nonnegative integer.

To simplify the problem, we assume the incident plane wave is linearly polarized, with the electric field in the x-direction and the magnetic field in the y-direction. Hence, $\mathbf{P}(t) = P_x(t)$ and $P_x^{n+0.5}$ is calculated as

$$\begin{aligned} P_x^{n+0.5} &= \frac{e}{p_F}A_x^{n+0.5} = \frac{e}{p_F}\int_{0.5\Delta t}^{(n+0.5)\Delta t} E_x(t')dt' \\ &= \frac{e}{p_F}\Delta t\sum_{m=0.5}^{n+0.5} E_x^m \end{aligned} \tag{5}$$

where m represents a half-integer step time. $J_{sx}^{n+0.5}$ can be calculated by substituting (5) into (1).

It is noted that (5) requires electric fields at half-integer time-steps. However, the values of electric fields are only calculated at integer time-steps [see (4)]. Therefore, an electric field at a half-integer time-step is approximated as the average value of its nearest two integer time-steps. Thus

$$\sum_{m=0.5}^{n+0.5} E_x^m = \frac{1}{2}\left(\sum_{m=0}^{n} E_x^m + \sum_{m=1}^{n+1} E_x^m\right). \tag{6}$$

To simplify the above expression, the auxiliary element B_x^n is defined as

$$B_x^n = \sum_{m=0}^{n} E_x^m. \tag{7}$$

Hence, it is easy to achieve the following updating equation by substituting (7) into (6):

$$B_x^{n+1} = B_x^n + E_x^{n+1}. \tag{8}$$

According to (6)–(8), (5) can be rewritten as

$$P_x^{n+0.5} = \frac{e\Delta t}{2p_F}\left(2B_x^n + E_x^{n+1}\right) \tag{9}$$

where E_x^{n+1} is the only unknown in order to determine $P_x^{n+0.5}$.

By substituting (1), (2), and (9) into (4), the updating equation of E_x can be expressed as

$$\begin{aligned} &E_x^{n+1}(i,j,k) \\ &\quad = E_x^n(i,j,k) \\ &\qquad + \frac{\Delta t}{\varepsilon}\left[\frac{H_z^{n+0.5}(i,j+0.5,k) - H_z^{n+0.5}(i,j-0.5,k)}{\Delta y}\right. \\ &\qquad\quad \left. - \frac{H_y^{n+0.5}(i,j,k+0.5) - H_y^{n+0.5}(i,j,k-0.5)}{\Delta z}\right] \\ &\qquad - \frac{\Delta t}{\varepsilon\Delta z}\frac{ev_F p_F^2}{\pi\hbar^2} \times \frac{P_x^{n+0.5}(i,j,k)}{\sqrt{1+\left(P_x^{n+0.5}(i,j,k)\right)^2}} \\ &\qquad \times \left[1 + \frac{3}{32}\left(\frac{2P_x^{n+0.5}(i,j,k)}{1+\left(P_x^{n+0.5}(i,j,k)\right)^2}\right)^2\right. \\ &\qquad\quad \left. + \frac{35}{1024}\left(\frac{2P_x^{n+0.5}(i,j,k)}{1+\left(P_x^{n+0.5}(i,j,k)\right)^2}\right)^4\right]. \end{aligned} \tag{10}$$

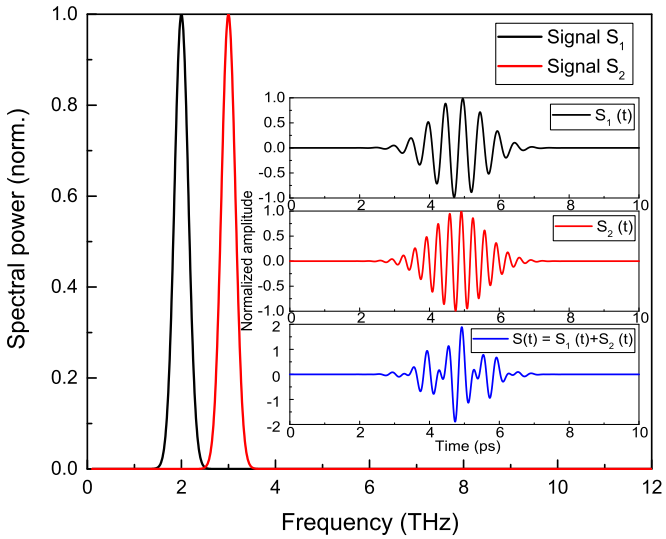

Fig. 2. Normalized spectral power of two incident signals S_1 and S_2. The inset is the temporal amplitudes of S_1, S_2 and $S_1 + S_2$, which are normalized to E_0.

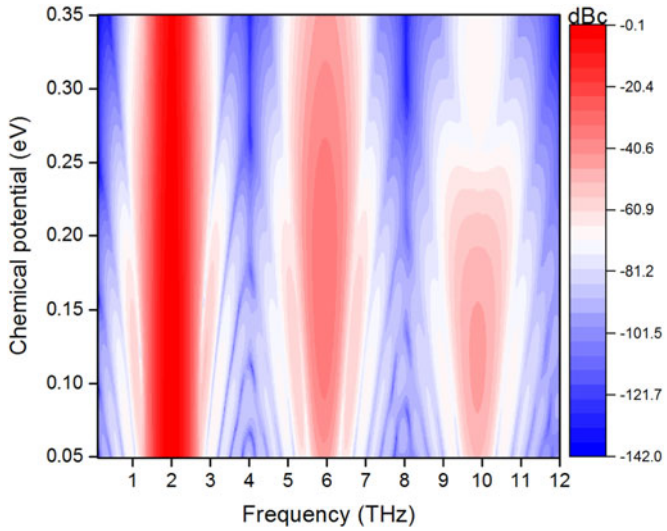

Fig. 3. Normalized spectral power of the transmitted wave that demonstrates odd-harmonic generation. The incidence has a 2 THz central frequency. The generated fundamental, third, and fifth harmonics are emphasized by the red color with darkness representing their strength. Various chemical potentials of graphene are taken into account.

This updating equation can be solved with the Newton–Raphson method.

III. Results and Discussion

The continuous graphene layer with periodic boundary condition is simulated to analyze the nonlinearity of large-area graphene. A uniform plane wave with normal incidence is used, and perfectly matched layers are employed in the propagation (z) direction. For simplicity, it is assumed that graphene is suspended in the air. The dimensions of FDTD cells are set as $\Delta x = \Delta y = \Delta z = 0.1$ μm corresponding to $1/250$ of the wavelength of the highest simulation frequency (12 THz). This small cell size is capable of providing converged simulation results, and the time-step is defined according to Courant's stability condition as [23]

$$\Delta t \leq \frac{1}{c\sqrt{\frac{1}{(\Delta x)^2}+\frac{1}{(\Delta y)^2}+\frac{1}{(\Delta z)^2}}}. \tag{11}$$

Two scenarios are simulated in this study: the odd-harmonic generation and the frequency-mixing effect. In the former scenario, a sine-modulated Gaussian signal $S_1(t)$ is used as the incident signal. For the latter case, an additional sine-modulated Gaussian signal $S_2(t)$, at a different frequency, is used. The two signals $S_{1,2}(t)$ are expressed as

$$S_{1,2}(t) = E_0 \sin\left(2\pi f_{c1,2}(t-t_0)\right) \mathrm{e}^{-\left(\frac{t-t_0}{\tau}\right)^2} \tag{12}$$

where E_0 is the temporal peak of the Gaussian pulse, $f_{c1,2}$ are the carrier frequencies ($f_{c1} = 2$ THz and $f_{c2} = 3$ THz), $t_0 = 4.8$ ps, and $\tau = 1$ ps. Fig. 2 presents the two signals in both frequency and time domains.

For the simulations of odd-harmonic generation, the plane wave consisting of only $S_1(t)$ is used. Due to the odd-harmonic generation, the primary 2 THz component should not be exclusively excited; the higher-order 6 and 10 THz components are also expected in the transmitted spectrum. The power spectrum

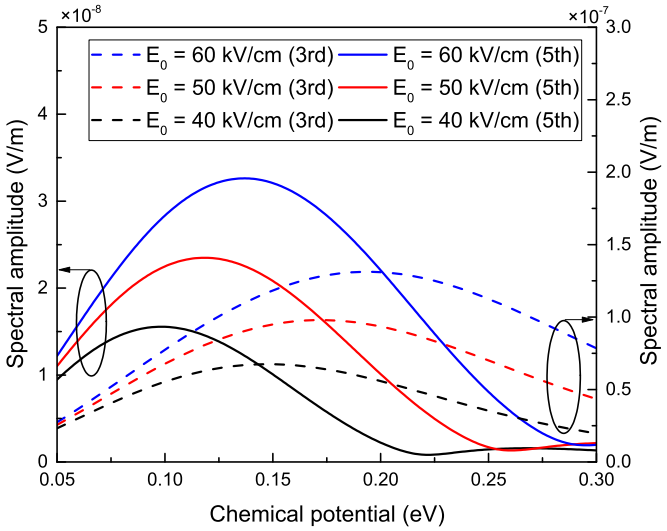

Fig. 4. Spectral amplitudes of third-harmonic generation at 6 THz and fifth-harmonic generation at 10 THz under three incidences with different values of E_0: 40 kV/cm, 50 kV/cm, and 60 kV/cm.

of the transmitted waves, plotted in Fig. 3, is defined as

$$P_{dBc} = 20\log_{10}\frac{E_{\text{trans}}(\omega)}{E_{\text{inc}}(2\,\text{THz})} \tag{13}$$

where $E_{\text{trans}}(\omega)$ is the amplitude of transmitted waves and $E_{\text{inc}}(2\,\text{THz})$ is the amplitude of incident waves at the carrier frequency 2 THz. The power spectrum clearly shows the generation of the third and the fifth harmonics.

Fig. 4 shows the spectral amplitudes of the third-order (6 THz) and fifth-order (10 THz) harmonics against the chemical potential of graphene under various incident signal strengths. It can be found that there are optimized chemical potentials for THG and fifth-order harmonic generations (FHG), which vary with the strength of the incident signals, as summarized in Table I.

TABLE I
OPTIMIZED CHEMICAL POTENTIALS FOR ODD-HARMONIC GENERATION

E_0 (kV/cm)	μ(meV) in THG	μ(meV) in FHG
40	148	106
50	172	124
60	195	140

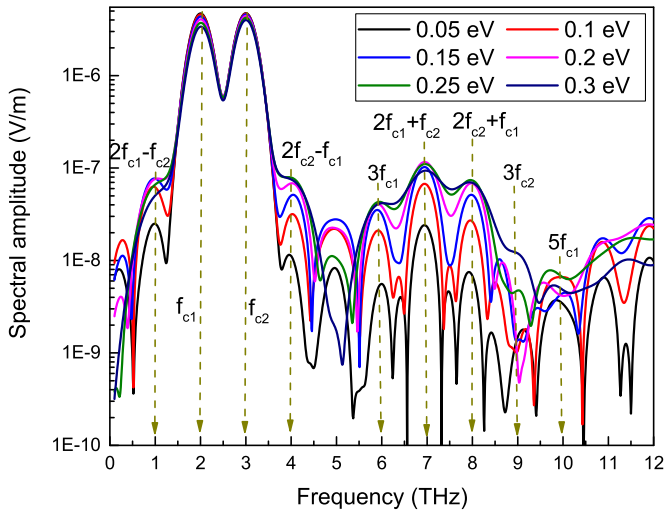

Fig. 5. Spectral amplitudes of transmitted signal through graphene for frequency-mixing effect. The incidence consists of two signals with central frequency at $f_{c1} = 2$ THz and $f_{c2} = 3$ THz, which is anticipated to generate third-order intermodulation harmonics (i.e., 1, 4, 7, and 8 THz) and other high-order harmonics due to mixing effect. Without loss of generality, odd-harmonic generations, such as 6, 9, and 10 THz, have also been shown in the figure. Chemical potential of graphene is tuned from 0.05 to 0.3 eV with the step 0.05 eV.

Another nonlinear phenomenon, the frequency-mixing effect, is also demonstrated with the proposed FDTD simulation. Two linearly x-polarized plane waves, as shown in Fig. 2, are used to explore the frequency-mixing effect. The two incident signals are summed up directly in the time domain (i.e., $S_{tot}(t) = S_1(t) + S_2(t)$) [24], and the spectral amplitudes of waves transmitted through graphene for various chemical potentials are illustrated in Fig. 5, where the resultant third-order intermodulation harmonics (i.e., $2f_{c1} \pm f_{c2}$ and $2f_{c2} \pm f_{c1}$) are clearly shown.

It is worth mentioning that in the FDTD simulations discussed above, graphene is a uniform layer. As the J–E characteristic formula [i.e., (1)] was derived independently of the graphene geometry, the proposed method holds the capability of simulating more complex graphene geometries.

IV. CONCLUSION

A novel FDTD modeling method has been proposed to model the nonlinear electrodynamic properties of graphene at THz frequencies. FDTD results demonstrate odd-harmonic generations as well as frequency-mixing effects in wave transmission through graphene. The effects of chemical potential are also investigated, and the proposed modeling method is expected to support the design of graphene-based nonlinear devices.

REFERENCES

[1] E. Carrasco, M. Tamagnone, and J. Perruisseau-Carrier, "Tunable graphene reflective cells for THz reflectarrays and generalized law of reflection," *Appl. Phys. Lett.*, vol. 102, no. 10, 2013, Art. no. 104103.
[2] B. Wu *et al.*, "Experimental demonstration of a transparent graphene millimetre wave absorber with 28% fractional bandwidth at 140 GHz," *Sci. Rep.*, vol. 4, 2014, Art. no. 4130.
[3] M. Tamagnone *et al.*, "Near optimal graphene terahertz non-reciprocal isolator," *Nature Commun.*, vol. 7, 2016, Art. no. 11216.
[4] M. Sprinkle *et al.*, "First direct observation of a nearly ideal graphene band structure," *Phys. Rev. Lett.*, vol. 103, no. 22, 2009, Art. no. 226803.
[5] S. Mikhailov and K. Ziegler, "Nonlinear electromagnetic response of graphene: Frequency multiplication and the self-consistent-field effects," *J. Phys., Condens. Matter*, vol. 20, no. 38, 2008, Art. no. 384204.
[6] A. Wright, X. Xu, J. Cao, and C. Zhang, "Strong nonlinear optical response of graphene in the terahertz regime," *Appl. Phys. Lett.*, vol. 95, no. 7, 2009, Art. no. 072101.
[7] V. A. Margulis, E. Muryumin, and E. Gaiduk, "Frequency dependence of optical third-harmonic generation from doped graphene," *Phys. Lett. A*, vol. 380, no. 1, pp. 304–310, 2016.
[8] I. Al-Naib, M. Poschmann, and M. M. Dignam, "Optimizing third-harmonic generation at terahertz frequencies in graphene," *Phys. Rev. B*, vol. 91, no. 20, 2015, Art. no. 205407.
[9] N. Savostianova and S. Mikhailov, "Giant enhancement of the third harmonic in graphene integrated in a layered structure," *Appl. Phys. Lett.*, vol. 107, no. 18, 2015, Art. no. 181104.
[10] S. A. Mikhailov, "Quantum theory of the third-order nonlinear electrodynamic effects of graphene," *Phys. Rev. B*, vol. 93, no. 8, 2016, Art. no. 085403.
[11] E. Hendry, P. J. Hale, J. Moger, A. Savchenko, and S. Mikhailov, "Coherent nonlinear optical response of graphene," *Phys. Rev. Lett.*, vol. 105, no. 9, 2010, Art. no. 097401.
[12] X. Yao and A. Belyanin, "Nonlinear optics of graphene in a strong magnetic field," *J. Phys., Condens. Matter*, vol. 25, no. 5, 2013, Art. no. 054203.
[13] P. Bowlan, E. Martinez-Moreno, K. Reimann, T. Elsaesser, and M. Woerner, "Ultrafast terahertz response of multilayer graphene in the nonperturbative regime," *Phys. Rev. B*, vol. 89, no. 4, 2014, Art. no. 041408.
[14] H. A. Hafez *et al.*, "Nonlinear terahertz field-induced carrier dynamics in photoexcited epitaxial monolayer graphene," *Phys. Rev. B*, vol. 91, no. 3, 2015, Art. no. 035422.
[15] R. Luebbers, K. Kumagai, S. Adachi, and T. Uno, "FDTD calculation of transient pulse propagation through a nonlinear magnetic sheet," *IEEE Trans. Electromagn. Compat.*, vol. 35, no. 1, pp. 90–94, Feb. 1993.
[16] R. Holland, "FDTD analysis of nonlinear magnetic diffusion by reduced c," *IEEE Trans. Antennas Propag.*, vol. 43, no. 7, pp. 653–659, Jul. 1995.
[17] P. M. Goorjian and A. Taflove, "Direct time integration of Maxwell's equations in nonlinear dispersive media for propagation and scattering of femtosecond electromagnetic solitons," *Opt. Lett.*, vol. 17, no. 3, pp. 180–182, 1992.
[18] R. M. Joseph and A. Taflove, "FDTD Maxwell's equations models for nonlinear electrodynamics and optics," *IEEE Trans. Antennas Propag.*, vol. 45, no. 3, pp. 364–374, Mar. 1997.
[19] M. Fujii, M. Tahara, I. Sakagami, W. Freude, and P. Russer, "High-order FDTD and auxiliary differential equation formulation of optical pulse propagation in 2-D Kerr and Raman nonlinear dispersive media," *IEEE J. Quantum Electron.*, vol. 40, no. 2, pp. 175–182, Feb. 2004.
[20] C. M. Reinke *et al.*, "Nonlinear finite-difference time-domain method for the simulation of anisotropic, $\chi^{(2)}$, and $\chi^{(3)}$ optical effects," *J. Lightw. Technol.*, vol. 24, no. 1, pp. 624–634, Jan. 2006.
[21] A. M. Attiya, "Modeling nonlinear electrical conductivity of graphene by using finite difference time domain," in *Proc. IEEE 33rd Nat. Radio Sci. Conf.*, 2016, pp. 340–347.
[22] Z. Kancleris, G. Slekas, and A. Matulis, "Modeling of two-dimensional electron gas sheet in FDTD method," *IEEE Trans. Antennas Propag.*, vol. 61, no. 2, pp. 994–996, Feb. 2013.
[23] A. Taflove and S. C. Hagness, *Computational Electrodynamics: The Finite-difference Time-Domain Method*. Norwood, MA, USA: Artech House, 2005.
[24] S. Mikhailov, "Theory of the nonlinear optical frequency mixing effect in graphene," *Phys. E, Low-Dimensional Syst. Nanostruct.*, vol. 44, no. 6, pp. 924–927, 2012.